The laser diagnostics of endometrial patology in case of uterine fibromioma

Peresunko O.P., Omar Kamal Numan, Ushenko A.G.
Bukovyna state medical university (Chernivtsi).

ABSTRACT

The paper presents the results of polarization-correlation investigation of multifractal collagen structure of physiologically normal and pathologically changed tissues of women's reproductive sphere. The technique of polarization selection of coherent biotissues' images with the following determination of their autocorrelation functions and spectral densities is suggested. The correlation-optical criteria of early diagnostics of pathological changes' appearance of myometry (forming of the germ of fibromyoma) and of uterine cervix (precancerous) are determined. The suggested paper is directed to investigation of the possibilities of pathological changes of biotissues' morphological structure by means of determining the polarizationally filtered autocorrelation functions (ACF) and corresponding spectral densities of their coherent images.

Keywords: laser, polarization, correlation, biotissue, uterine cervix, diagnostics, precancerous, myoma

1. INTRODUCTION

The structure of the majority of tissues can be regarded as double-component amorphously (intermediate substance)-crystalline (optically uniaxial collagen fibers) matrix[1-5]. The analysis of pathological changes of such a structure shows that these changes appearance can be defined as:
tumor formation of soft tissues of woman's reproductive sphere (WRS) with forming of collagen multifractal nets' growth directions[6];
statistic excrescence of uterine cervix structure[7].

Tissue probing by coherent light leads to the formation of optical signal:

$$S(X,Y) = I(X,Y) + U(X,Y), \tag{1}$$

there $U(X, Y)$ and $I(X, Y)$ – random and "anisotropic" components of object field. The autocorrelation function of the detected optical signal can be defined by following relation (one-dimensional case is analyzed for simplicity without loss of generality)[8]:

$$G_{xx}(\Delta x) = \lim_{X_0 \to \infty} \frac{1}{X_0} \int_0^{X_0} [I(X) + U(X)][I(X - \Delta X) + U(X - \Delta X)]dx. \tag{2}$$

This expression can be transformed to the following form:

$$G_{xx}(\Delta x) = G_{II}(\Delta x) + G_{IU}(\Delta x) + G_{UI}(\Delta x) + G_{UU}(\Delta x). \tag{3}$$

In the case of statistically independent signal I(X) and noise U(X) components we can rewrite Eq. 4 as follows:

$$G_{xx}(\Delta x) = G^{*}{}_{II}(\Delta x) + G^{*}{}_{UU}(\Delta x) + G^{\otimes}{}_{II}(\Delta x) + G^{\otimes}{}_{UU}(\Delta x). \tag{4}$$

Correlation terms $G^{\otimes}{}_{II}(\Delta x), G^{\otimes}{}_{UU}(\Delta x)$ fall to zero with the increasing interval of integration X_0. Finally, we have

$$G_{xx}(\Delta x) = G^{*}{}_{II}(\Delta x) + G^{*}{}_{UU}(\Delta x). \tag{5}$$

The component $G^{*}{}_{UU}(\Delta X)$ plays the role of a noise component in the course of $G_{xx}(\Delta X)$ definition and makes insufficiently effective the diagnostical value of $G^{*}{}_{II}(\Delta X)$. This problem can be solved by polarization selection of coherent image of a diagnosed tissue.

The polarization features of biofractals can be totally described by the following Mueller matrix[9,10]:

$$\|F\| = \begin{Vmatrix} 1 & 0 & 0 & 0 \\ 0 & f_{22} & f_{23} & f_{24} \\ 0 & f_{32} & f_{33} & f_{34} \\ 0 & f_{42} & f_{43} & f_{44} \end{Vmatrix}, \tag{6}$$

where:

$$\begin{aligned} f_{22} &= \cos^2 2\rho + \sin^2 2\rho \cdot \cos\delta; \\ f_{23} &= f_{32} = \cos 2\rho \sin 2\rho (1 - \cos\delta); \\ f_{24} &= -f_{42} = -\sin 2\rho \sin\delta; \\ f_{33} &= \sin^2 2\rho + \cos^2 2\rho \cos\delta; \\ f_{34} &= -f_{43} = \cos 2\rho \sin\delta; \\ f_{44} &= \cos\delta. \end{aligned} \tag{7}$$

In these equations, the magnitude ρ is the angle of orientation of the fractal domain optical axis with respect to the incidence plane, and δ is the induced phase shift. As a result of linearly polarized laser beam propagation through an element of multifractal collagen net, an object field is induced with following values of the azimuth α and the polarization ellipticity β:

$$\begin{aligned} \alpha &= 0{,}5 \arctan\left(\frac{f_{23}\cos 2\alpha_0 + f_{13}\sin 2\alpha_0}{f_{22}\cos 2\alpha_0 + f_{23}\sin 2\alpha_0}\right); \\ \beta &= 0{,}5 \arcsin(f_{42}\cos 2\alpha_0 + f_{43}\sin 2\alpha_0) \end{aligned} \tag{8}$$

Here α_0 is the polarization azimuth of illuminating laser beam. It can be seen that the image contrast of a fractal fragment against the background of an amorphous substance will be determined by the following equation:

$$K(\alpha_0, \Theta) = \frac{I_+ - I_-}{I_+ + I_-} = \frac{A - \Delta I \cdot B}{A + \Delta I \cdot B}, \tag{9}$$

where

$$\Delta I = \frac{I_0}{a^2}, \tag{10}$$

$$A = \cos^2(\alpha - \Theta) + \tan^2\beta \sin^2(\alpha - \Theta), \tag{11}$$

$$B = \cos^2\Theta . \qquad (12)$$

Here I, I_0 are the intensities of background and object signals induced by amorphous and crystalline components of tissue for random value of the rotation angle of the polarization axis of analyzer Θ; I_0, a^2 – corresponding intensities in the case of $\Theta=0^\circ$.

Multifractal collagen structure of tissue in the plane of histological section possesses a wide variety of random values of the orientation ρ and the optical anisotropy δ, and, consequently, the coordinate-dependent polarization parameters $\alpha(X, Y)$; $\beta(X, Y)$ of boundary field. That's why the level of visualization of such a multifractal net in the coherent image will be determined as follows:

$$V_\Sigma(\Theta) = \sum_{\alpha=0}^{\pi} \sum_{\beta=0}^{\frac{\pi}{2}} V(Q_\alpha, W_\beta, \alpha, \beta). \qquad (13)$$

The computer simulation shows the wide range in which the visualization parameter $V(\sigma_\rho, \Theta)$ changes. The largest value is obtained when the rotation angle of the analyzer Θ is close to 90°. In this case, the object signal can be presented as:

$$S^*(X) = I^*(X) + I^{*0}(X), \qquad (14)$$

and autocorrelation function has the following form:

$$G^*(\Delta x) = \lim_{X_0 \to \infty} \frac{1}{X_0} \int_0^{X_0} Q_\alpha(\Delta x) W_\beta(\Delta x) \left\{ \sin^2\alpha(x) + \tan^2\beta(x)\cos^2\alpha(x) \right\} \left\{ \sin^2\alpha(x-\Delta x) + \tan^2\beta(x-\Delta x)\cos^2\alpha(x-\Delta x) \right\} dx \qquad (15)$$

Thus, this relation illustrates the possibilities of autocorrelation analysis of multifractal components in tissue coherent images. In the accordance with Wiener-Khintchin theorem[8], it is convenient to use the spectral density for characterization of such component:

$$J_{xx}(\nu_\rho) = \int_{-\infty}^{\infty} G^*_{xx}(\Delta x) \cos 2\pi\nu_\rho x dx, \qquad (16)$$

where ν_ρ is the spatial frequency. Analysis of obtained relations shows that appearance of pathological changes, leading to the formation of tissue multifractal collagen structure (tumor formation) is connected with appearance of oscillations of $G^*_{xx}(\Delta X)$ oscillations. As a result, a quasi-discrete spectrum $S_{xx}(\nu_\rho)$ appears. On the contrary, the overgrowth and de-orientation of the architectonic collagen net (psoriasis) will be manifested in smoothing $G^*_{xx}(\Delta X)$ and appearing continuous spectrum $S_{xx}(\nu_\rho)$.

2. EXPERIMENTAL SETUP

Figure 1 illustrates the scheme of experimental setup. The beam of He-Ne laser 1 (λ=0.6328 μm) is collimated by the lens system 2 and passes through the polarization unit (λ/4 plate 3 and polarizer 4) and after this falls on sample 5 which is placed in the cuvette with physiological solution 7. The objective 8 projects the coherent image of histological section through the analyzer 9 on CCD-camera connected with PC 11. The detected polarization images are digitized with use of 256 gray level scale; the image format was 800×600 pixels.

3. EXPERIMENTAL RESULTS

The following groups of tissue samples were investigated experimentally: histological sections of myometry (the WRS biotissue) – group A: histological sections of uterine cervix – group B. The thickness of samples was 10 μm that corresponded to the condition of a single scattering. Figure 2 presents images of such sections, obtained in the crossed (⇑⇒) polarizer and analyzer. Normal structure of tissues A and B is shown in figures 2a, 2d, while the figures 2b, 2c, 2e, and 2f present the pathologically changed tissues.

Coherent images of myometry tissue with probable fibromyoma node[6] (fragments 2b, 2c) are characterized by optically anisotropic collagen net being compared with normal tissue (fragment 2a). The precancerous state human uterine cervix collagen net (fragments 2e, 2f) is characterized by sufficient enlargement and disorientation in comparison with the healthy tissue (fragment 2d).

Figure 3 illustrates the series of ACF's for coherent images of myometry tissue with probable fibromyoma germ. These images were obtained for the following cases of analyzer axis orientation: 0°, 45° and 90° (figures 3a, 3b, 3c). The corresponding spectral densities are illustrated by graphs 3d, 3e, 3f. All autocorrelation function exhibit a peak in the origin that is related to white noise connected with random intensity fluctuations in tissue coherent image. One can observe the extrema assemblage on ACF tails. These peculiarities are associated with presence of quasi-periodic component in the structure of polarization images of multifractal net.

Figure 4 presents the results of the comparative polarization-correlation analysis of coherent images of normal (4a, 4b) and pathologically changed myometry tissue (4c, 4d). It can be seen that the correlation structure of polarization images of physiologically normal myometry does not contain any sufficiently marked fluctuation component. The fibromyoma germ forming is manifested in the increasing amplitude of fluctuations (in 1.8-2 times) of ACF tails and the extrema of quasi-discrete spectra $S_{XX}(\nu_\rho)$ of polarization images of multifractal collagen net.
Changes in polarization-dependent ACFs and spectral densities $S_{XX}(\nu_\rho)$ of intensity distributions for coherent images of human uterine cervix are illustrated by figure 5. The significant difference of auto-correlation peak half-width $G_{XX}^* - \Delta x_0$ (graphs 5a, 5b, 5c) and power spectra $S_{XX}(\nu_\rho=0)$ (fragments 5d, 5e, 5f) should be noted for analyzed coherent images of the derma layer. It is obvious that these tendencies are related to an increase of characteristic size of collagen structures. In its turn, this leads to the increase of correlation length Δx_0 and concentration of the intensity in polarization images of collagen structures in the vicinity of zero spatial frequency $\nu_\rho = 0$. Figure 6 displays the histograms of distribution of parameters Δx_0 and $S_{XX}(\nu_\rho=0)$ for coherent images of 38 samples of physiologically normal uterine cervix and 41 samples of the pre-cancerous uterine cervix.

4. SUMMARY

The presented results show the potentiality of the polarization correlometry of the tissue coherent images for diagnostical applications. The study of polarization-correlation structure of tissue object fields gives the possibility:
1. to determine the stochastic quasi-periodic component in tissue coherent images, which is identified with the orientated structure of tissue multifractal net;
2. to define the spatial-frequency structure of optically anisotropic fractal component of biotissue;
3. to diagnose the appearance and dynamics of the progress of pathological changes in morphological structure of tissue collagen nets.

REFERENCES

1. B.Mandelbrot , *The Fractal Geometry of Nature*, New York: Freeman, 1983
2. R. Nossal, J. Kiefer, G.H. Weiss *et al.*, *Appl.Opt.*, **27**, 3382, **1988**.
3. W.F. Cheong, S.A. Prahl, , and A.J. Welch, *IEEE J. Quantum Electron.*, **26**, 2166, 1990.
4. V.V. Tuchin, *Proc. SPIE*, **1884**, 234, 1993.
5. V.V. Tuchin, , *Usp. Fiz. Nauk*, № 5, 517, 1997

6. E.M. Vikhlyaeva, *Manual on Endocrine Gynecology,* Moscow, in Russian, p. 765, 1997
7. G. Raikh, *Collagen,* Moscow, p. 328, 1969.
8. A.V. Opptnheim, R.W. Sehafer, *Digital SignalProcessing,* Prentice Hall, p. 435, 1975.
9. A.G. Ushenko, *Proc. SPIE*, **3317**, p.331, 1997.
10. V.P. Pishak, A.G. Ushenko, , *SPIE Proc.*, **3317**, p.418, 1997.

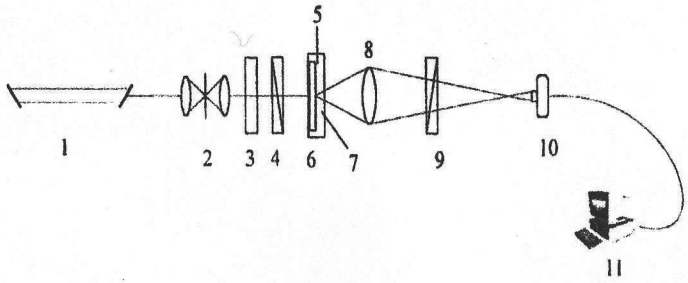

Figure 1: Optical scheme of the experiment.

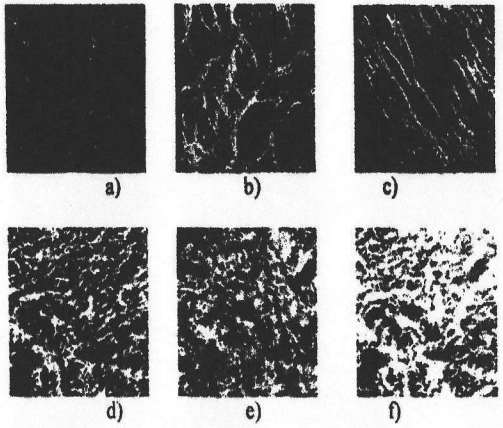

Figure2: Coherent images of WRS (Women Reproductive Sphere) myometry and uterine cervix.

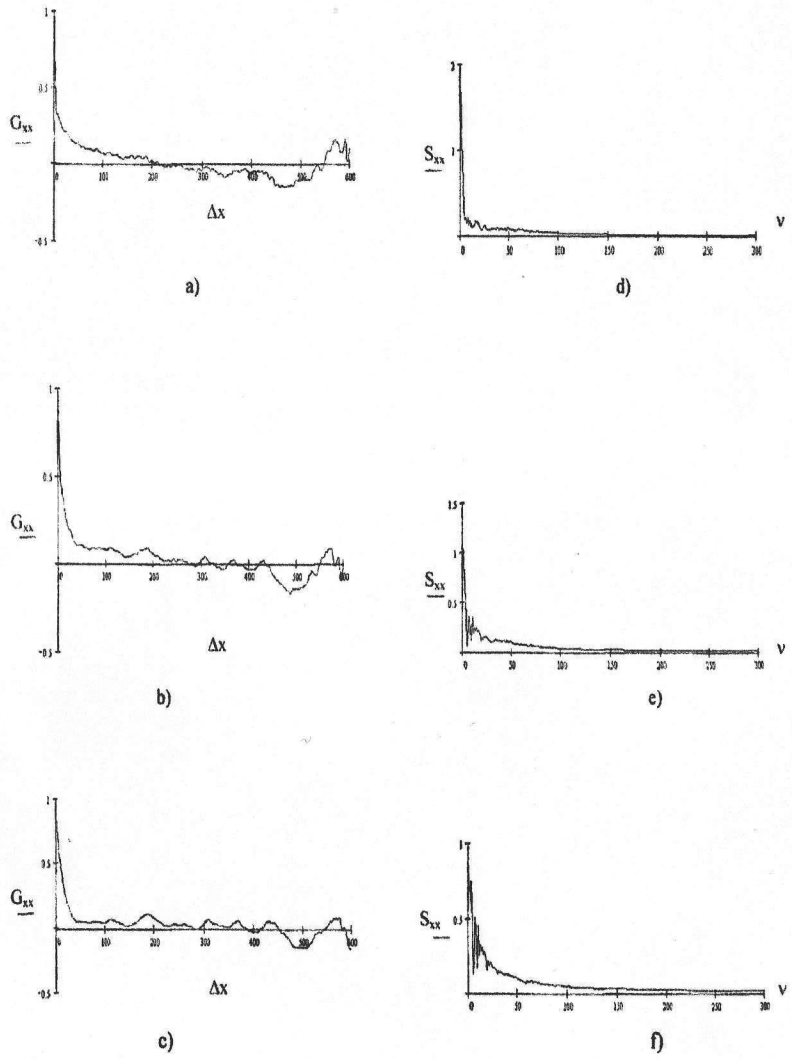

Figure 3: The dynamics of polarization changes in the ACF and spectral densities of coherent image of myometry with the probable fibromyoma germ.

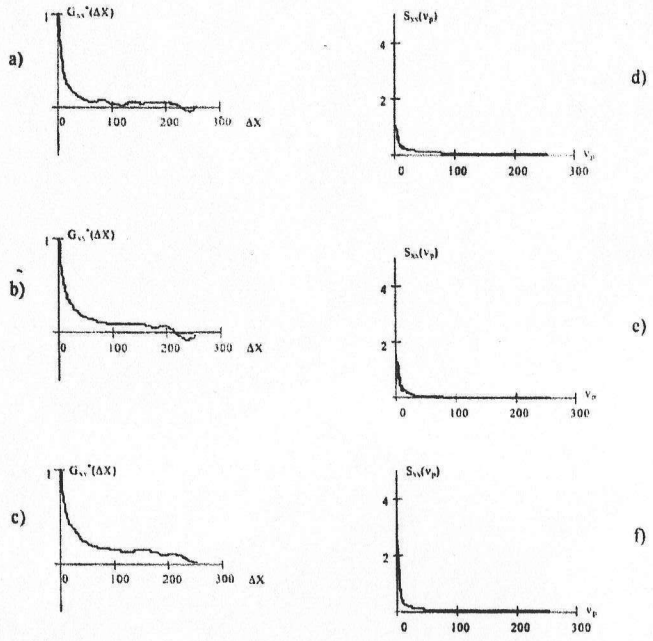

Figure 5: Polarization-correlation structure of uterine cervix coherent images in the normal and pathological states.

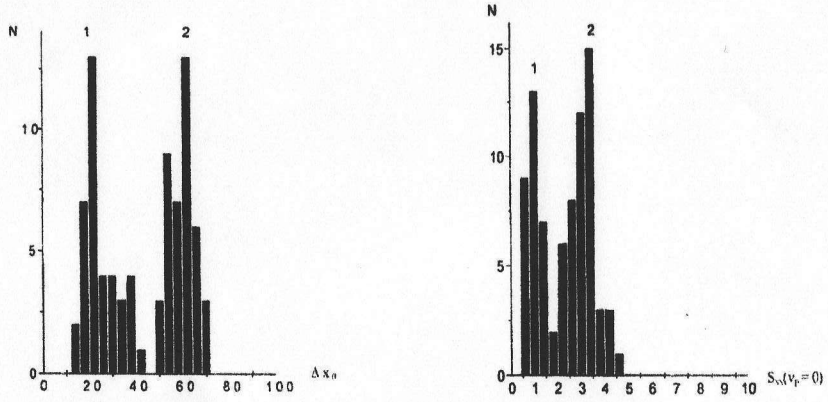

Fig.8. The probability structure of the ACF (a) and spectral densities (b) of uterine cervix coherent images. 1 – the histograms of physiologically normal tissue; 2 – the histograms for precancerous uterine cervix.